Practical Papers, Articles and Application Notes

Kye Yak See, Technical Editor

With the advancements of robotic technology, robots have been widely deployed in factory automation and health care. One of the major applications of robots in health care is the myoelectric artificial hand. It consists of a myoelectric signal detector connected to a motor-controlled artificial hand driving unit by wires. In the near future, they will be connected wirelessly for convenience but this may pose an EMI risk to the normal operation of the artificial hand. One possible source of EMI is the electrostatic discharge (ESD) from a charged human body. As the malfunction of a myoelectric artificial hand due to ESD has a direct impact on human life, high immunity performance is required. Yasuhiro Morinaga, Keinosuke Nagai, Jianqing Wang, and Daisuke Anzai from Nagoya Institute of Technology, Japan, look into this impact and propose design improvements to enhance the immunity of the myoelectric artificial hand against ESD in the paper "Impact of Electrostatic Discharge on Wearable Robotic Hand and Improvement of Immunity Performance by Wireless Control."

The growth of wirelessly-enabled medical devices are driven by advances in wireless technologies. However, incorporating wireless technology in medical devices has to be implemented with care to ensure patient safety and device effectiveness. This is particularly relevant to technologies that operate in unlicensed spectrum bands, where Wi-Fi, Bluetooth and other technologies operate. A method to evaluate wireless coexistence of a medical device encompassing the risk assessment is presented in the second paper "A Case Study of Medical Device Wireless Coexistence Evaluation", contributed by Mohamad Omar Al Kalaa, Joshua Guag, and Seth J. Seidman from Center for Devices and Radiological Health, U.S. FDA; and Yao Ma and Jason Coder from National Institute of Standards and Technology (NIST).

Impulsive noise modeling is an important part in analyzing and designing communication systems. Man-made impulsive noise can be due to intentional information exchange such as short-burst transmissions with high power, as well as due to switching and industrial activities. The third and last paper "Using Open-Source Software Defined Radio Platforms for Empirical Characterization of Man-Made Impulsive Noise" describes the use of affordable software-defined radio (SDR) platforms for measuring and characterizing man-made noise with impulsive components. Otilia Popescu and Dimitrie C. Popescu from Old Dominion University, and John Musson from Thomas Jefferson National Accelerator Facility, elaborate on the parameters that characterize the Class A Middleton impulsive noise model and how they can be applied for modeling of distinct RF environments, such as a medium-density office workspace, an urban commute scenario, and a hospital campus.

This year is an unusual year, where the pandemic affects all of us, be it socializing with friends, traveling with family, and working from home. Nevertheless, let me take this opportunity wishing all a Wonderful Holiday Season and a Happy New Year. Do enjoy reading these three papers and I look forward to more interesting papers from you so that they benefit the EMC community. Please contact me at ekysee@ntu.edu.sg if you are having the thought of contributing a paper in this column.

Impact of Electrostatic Discharge on Wearable Robotic Hand and Improvement of Immunity Performance by Wireless Control

Yasuhiro Morinaga, Keinosuke Nagai, Jianqing Wang, Daisuke Anzai
Nagoya Institute of Technology, Japan

Abstract: Myoelectric artificial hand is a typical wearable robotic hand operated by motors based on detected myoelectric signals. A wired connection between the myoelectric signal detector and motor controller is currently the mainstream, but the wireless control is expected for convenience. In this study, focusing on a myoelectric artificial hand, we performed electrostatic discharge immunity tests based on IEC61000-4-2 to clarify the mechanism of malfunction with respect to electrostatic discharge noise. Using an optical electric field sensor, we investigated the correlation between the peak level, time duration, and energy of electric field generated by electrostatic discharge and the malfunction rate of myoelectric artificial hand. The measurement results showed that the malfunction of myoelectric artificial hand was strongly correlated with the peak electric field level, and the primary coupling location of electrostatic discharge noise on the myoelectric artificial hand was the wires between the myoelectric signal detector

The authors are with Graduate School of Engineering, Nagoya Institute of Technology, Gokiso-cho, Showa-ku, Nagoya 466-8555, Japan. e-mail: wang@nitech.ac.jp
This study was supported in part by JSPS KAKENHI Grant Number 19H02139.

and the motor controller. Based on these findings, we developed a wireless myoelectric artificial hand to remove the above-mentioned wires and to increase the convenience. As a result, compared to the wired control, the wireless myoelectric artificial hand exhibited a much higher immunity level for the electrostatic discharge noise. This is because the wires that were experimentally identified to pick up noise were replaced by a wireless link where a wideband modulation scheme resistant to electrostatic discharge type impulse noise was adopted.

Index Terms: Wearable robot, myoelectric artificial hand, electrostatic discharge, immunity test, wireless control.

I. Introduction

In recent years, wearable robots are attracting a lot of attention in the industrial, medical and health care fields [1]-[3]. Myoelectric artificial hand is one of the typical examples. A myoelectric artificial hand consists of a myoelectric signal detector and a motor-controlled artificial hand driving unit [4].

Currently they are connected by wires. However, it is expected to be wireless for convenience. On the other hand, a wide range of wireless technology applications have become a major cause of electromagnetic interference on various wearable robots. Electrostatic discharge (ESD) from charged human body can also affect the normal operation of myoelectric artificial hand [5]-[7] because it produces a sharply rising peak electric field and a very wide frequency component. Since malfunction of myoelectric artificial hand due to ESD may affect human life, high immunity performance is required. Although there are many studies related to ESD immunity to various electrical devices, only a few focus on wearable devices or robots where the electrical circuit units are on the human body. Ishida et al. measured the characteristics of discharge currents through body-attached metal for modeling ESD from a wearable device [8][9]. Kohani et al. evaluated the characteristics of ESD events in wearable medical devices in [10], and Liao et al. investigated an evaluation method for ESD-generated interference on bio-sensors in [11]. An experimental study of electrical stress of ESD on wearable devices was reported in [12]. The immunity performance of wearable devices and robots may vary greatly due to the presence of the human body. To clarify the mechanism of malfunction due to ESD in myoelectric artificial hand, we perform an immunity test under the IEC 61000-4-2 testing conditions. Since our main purpose is to clarify the mechanism of malfunction of myoelectric artificial hand, the tests focused on indirect ESD with a standard ESD gun for a vertical coupling plane. The IEC 61000-4-2 standard, however, only specifies a measurement position of 10 cm away from the vertical coupling plane for equipment under test (EUT). In view of that the electric field generated by ESD is not uniform on the vertical measurement plane of 10 cm away from the vertical coupling plane, the impact of ESD noise on the EUT may vary depending on the placement and orientation of the EUT.

In this study, we first measure the electric field distribution at the measurement plane using an optical electric field sensor. Then, using the myoelectric artificial hand as EUT, we extract various parameters such as peak level, time duration, and energy of the ESD-generated electric field pulse, and investigate the correlation characteristics of these parameters regarding the malfunction rate of myoelectric artificial hand at different positions and orientations for clarifying the determinant of malfunction of myoelectric artificial hand. Moreover, we attempt to identify the coupling location of ESD noise, and show that the most of ESD noises are coupled into the myoelectric artificial hand through the wires between the myoelectric signal detector and the motor controller. As a countermeasure, we propose a human body communication (HBC) [13][14] based wireless technology which employs a wideband impulse radio (IR) modulation scheme in the 10 - 50 MHz band [15]-[17] to remove the wires, and demonstrate its high immunity performance under the IEC61000-4-2 ESD testing conditions [18].

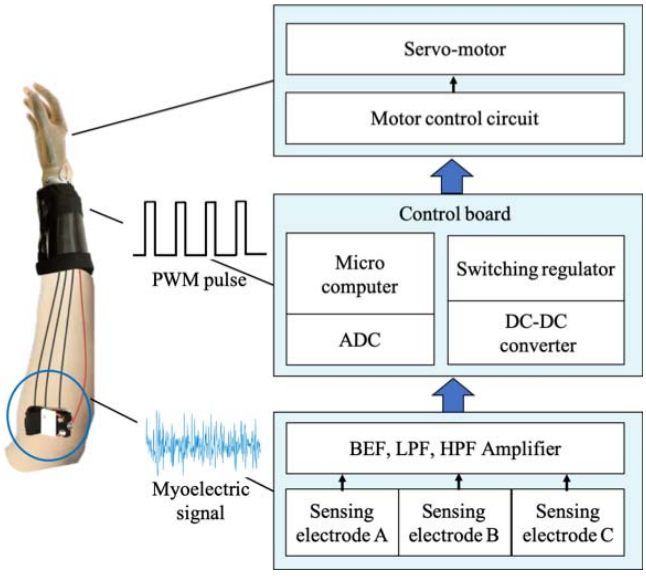

Fig.1. Block diagram of a myoelectric artificial hand.

This paper is organized as follows. Section II describes the specifications of the myoelectric artificial hand as an EUT. Section III investigates the dominant parameters of ESD-generated electric field that cause the malfunction of myoelectric artificial hand, and the position where the ESD noise is coupled. Section IV describes our developed wireless myoelectric artificial hand and shows higher immunity performance under the IEC61000-4-2 ESD testing conditions than the wired control. Section V concludes this study.

II. Myoelectric Artificial Hand

Fig. 1 shows a block diagram of myoelectric artificial hand used in this study as a typical wearable robotic hand. In order to control the myoelectric artificial hand, three myoelectric signals at the flexor digitorum superficialis muscle, extensor digitorum muscle and extensor pollicis longus muscle are used as shown in Fig. 2. The myoelectric artificial hand acquires these myoelectric signals using three pairs of sensing electrodes and a ground electrode for grounding the human body. The myoelectric signals acquired by the three pairs of sensing electrodes are first filtered and amplified, and then are sent to a controller board mounted in the myoelectric artificial hand. The controller board is equipped with three channel analog to digital converter (ADC) with a sampling frequency of 2 kHz and a quantization of 12 bits, and performs digital processing in a microcomputer to identify the signals. Rectified smoothing value and power spectrum are used as identification

functions in the microcomputer. The myoelectric artificial hand is pre-trained by a neural network using training data and then performs motion detection to determine motion commands that characterize the current input myoelectric signal. The identified motion command takes pulse width modulation (PWM) signal form and is output to the servo motor for operating the myoelectric artificial hand. In this way, the myoelectric artificial hand moves according to the motion command generated from the detected myoelectric signals.

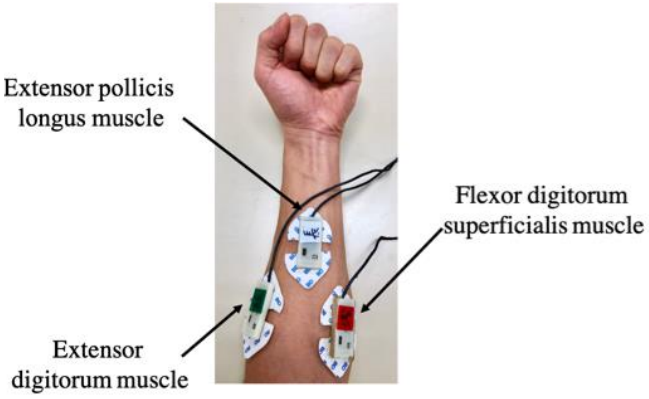

Fig.2. Detection of three myoelectric signals used to control a myoelectric artificial hand.

III. Mechanism of Malfunction of Myoelectric Artificial Hand Under ESD Test Environment

Since the myoelectric artificial hand is attached to the human body, it is assumed to be vulnerable to electromagnetic interference such as ESD noise, and a high immunity performance to ESD is required. However, the current IEC61000-4-2 standard does not specify how to simulate the human body during wearable device testing. It also does not specify the detailed position of EUT during indirect ESD testing. If the electromagnetic field generated from a vertical coupling plane is not uniform, the impact on the EUT will depend on the test arrangement. Therefore, in this study, we employed an arm-shaped gel phantom to simulate the actual human arm for testing the malfunction of myoelectric artificial hand. This system has already been reported in [7] and shown to be valid. In addition, to clarify the mechanism of malfunction of the myoelectric artificial hand, we first measured the electric field distribution near the vertical coupling plane under IEC61000-4-2 test conditions. Then we extracted the peak level, time duration and energy from the measured ESD-generated electric field pulse. By comparing the correlation between the malfunction rate of myoelectric artificial hand and the extracted parameters of ESD-generated electric field pulse, the dominant parameter causing malfunction of myoelectric artificial hand was determined.

A. Electric Field Measurement

Fig. 3 shows the measurement environment of indirect ESD based on IEC 61000-4-2, which consists of a wooden table, a vertical coupling plane, a horizontal coupling plane, and an ESD gun. An optical electric field sensor head (Seiko Giken, CS-1210) was connected to an optical electric field sensor controller (Seiko Giken, C3-1055) and a digital oscilloscope (Tektronix, TDS6604) with a sampling rate of 20 GS/s and a frequency bandwidth of 6 GHz to measure the electric field generated when the ESD gun discharges to the vertical coupling plane. The measurement plane was a vertical plane which is 10 cm or 45 cm away from the vertical coupling plane. The height and position of the optical electric field sensor head was adjusted at the measurement planes by attaching it to a polystyrene foam. Table I shows the measurement conditions.

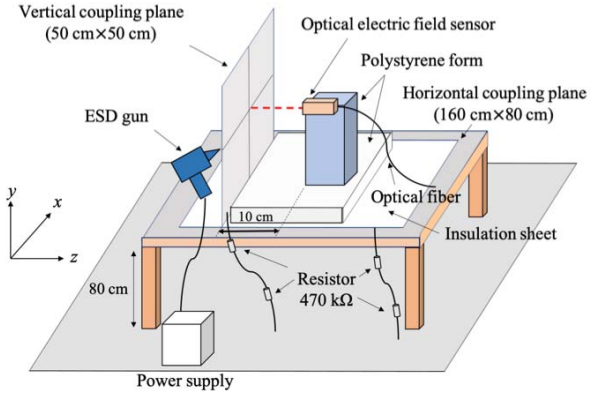

Fig. 3. Electric field measurement environment of indirect ESD.

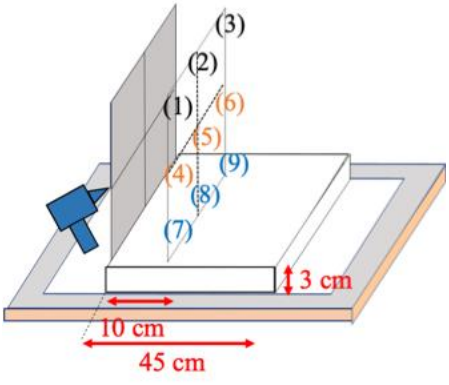

Fig. 4. Electric field measurement positions.

TABLE 1
MEASUREMENT CONDITIONS OF ESD-GENERATED ELECTRIC FIELD

Discharge method	Contact discharge
Charging voltage	_±2, _±4 kV
Coupling plane	Vertical plane
Time interval of discharge	0.05 s
Number of discharge	999
Distance from vertical coupling plane	10, 45 cm
Number of measurement positions	9
Electric field component	x, y, z

The measurement was under an indirect discharge test condition by bringing the charged ESD gun to contact with the vertical coupling plane. The ESD gun charging voltage was 2 or 4 kV, the discharge interval was 0.05 seconds, and the number of discharge was 999 times in total. As shown in Fig. 4, the measurement positions were 9 positions on the measurement planes 10 cm or 45 cm away from the vertical coupling plane. At each measurement position, the three electric field components, i.e., the x, y, and z components were measured.

Fig. 5 shows an example of pulse voltage waveform measured using the optical electric field sensor, where Vmax is the peak

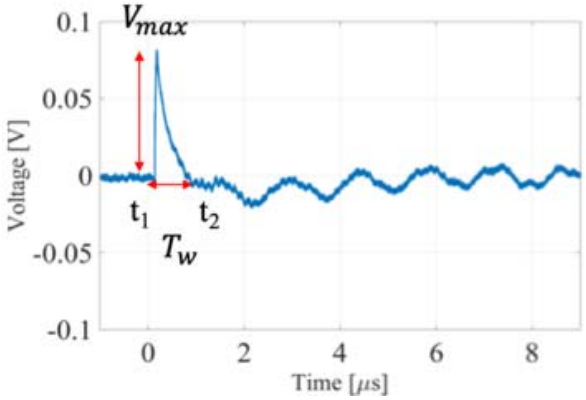

Fig. 5. Example of ESD-generated pulse voltage measured by the optical electric field sensor.

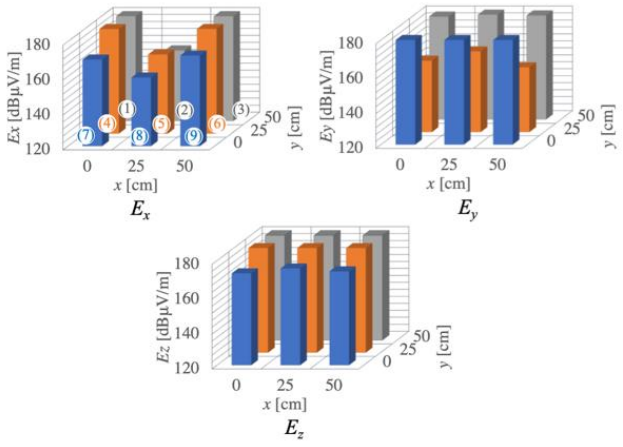

Fig. 6. Peak level distribution of pulse electric field at the measurement plane 10 cm away from the vertical coupling plane. The ESD gun charging voltage is 4 kV.

voltage level, *t1* and *t2* are the zero crossing points for determining the time duration *Tw* of pulse. From the measurement results using the optical electric field sensor, it was found that the polarity and peak level of the ESD-generated pulse differ depending on the measurement positions, field components, and ESD gun charging voltage. In order to investigate the dominant parameters for malfunction of the myoelectric artificial hand, we calculated the peak level, time duration and energy of the ESD-generated electric field at the 9 measurement positions. Figs. 6, 7 and 8 show the distributions of peak level, time duration, and energy of pulse electric field, respectively, when the ESD gun charging voltage is 4 kV and the measurement plane is 10 cm away from the vertical coupling plane. The peak level E_P of electric field strength was obtained by

$$E_P[\mathrm{dB}\mu\mathrm{V/m}] = \mathrm{V_{max}}[\mathrm{dB}\mu\mathrm{V}] + \mathrm{AF}[\mathrm{dB/m}] \quad (1)$$

$$T_W = t_2 - t_1 \quad (2)$$

and the energy of pulse was obtained by

$$U = \sum_{t=t_1}^{t_2} V^2(t) \quad (3)$$

where t_1 was the first zero crossing timing from *Vmax* to the left side, and t_2 is the first zero crossing timing from *Vmax* to the right side in Fig. 5. It should be also noted that the energy obtained from (3) is actually for a resistance of 1 Ω.

Comparing the peak electric field components on the left side (measurement positions 1, 4, 7), center part (measurement positions 2, 5, 8) and right side (measurement positions 3, 6, 9) of Fig. 4, *Ex* was found to have almost the same peak level on the left side and right side at all heights, approximately 15 dB higher at maximum than that on the center part. Conversely, the peak level of *Ey* on the center part (measurement positions 2, 5, 8) was higher than that on the left and right sides, and the difference was 1 - 7 dB. For the peak level of *Ez*, it was confirmed to have a difference of 1 - 2 dB on the left side, center part and right side, so *Ez* has a relatively uniform peak field strength compared to other field components. In addition, *Ex* and *Ez* have the almost same peak level at the top (measurement positions 1, 2, 3) and middle (measurement positions 4, 5, 6) of the measurement plane. At the bottom (measurement positions 7, 8, 9) of measurement plane they were found to be about 10 dB lower compared to that at the top and middle. On the other hand, *Ey* was the weakest at the middle (measurement positions 4, 5, 6), about 15 dB lower than that at the top and bottom of measurement plane.

When the ESD gun charging voltage was ±2 kV, the distribution of peak level of electric field was similar to the case of ±4 kV. But the peak level was about 5 dB lower at all measurement positions. When the measurement plane was moved to 45 cm away from the vertical coupling plane, the peak level of electric field was found to be more than 10 dB lower than when it was 10 cm away from the vertical coupling plane. The shape of the peak level distribution at the two measurement planes was similar, although at some measurement positions it showed different trends. In terms of the time duration and energy of measured ESD-generated pulse electric field, they also depend on the field component, measurement position and distance from the vertical coupling plane. As shown in Fig. 7, the characteristics of time duration are not exactly the same as the peak level of electric field, but in most cases the higher the peak level, the longer the time duration is. Moreover, in Fig. 8, the high peak level and longtime duration of the pulse electric field generate more energy. As such, any of the parameters has the possibility to dominate the immunity test results.

B. Immunity Test of Myoelectric Artificial Hand

From the electric field measurement results, it was confirmed that the ESD-generated electric field under the IEC61000-4-2 test conditions differs depending on the field component and measurement position. So, the malfunction rate should vary at different positions and orientations. We performed an immunity test under the IEC61000-4-2 test conditions to confirm this perspective.

Fig. 9 shows the ESD immunity test environment. In the immunity test, three myoelectric signals were generated using a pseudo biological signal generator [7] and sent to three pairs of input electrodes embedded in an arm-shaped biological- equivalent gel

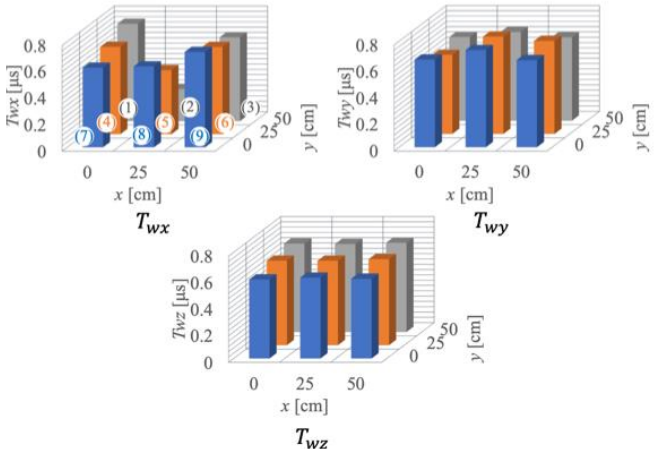

Fig. 7. Time duration distribution of pulse electric field at the measurement plane 10 cm away from the vertical coupling plane. The ESD gun charging voltage is 4 kV.

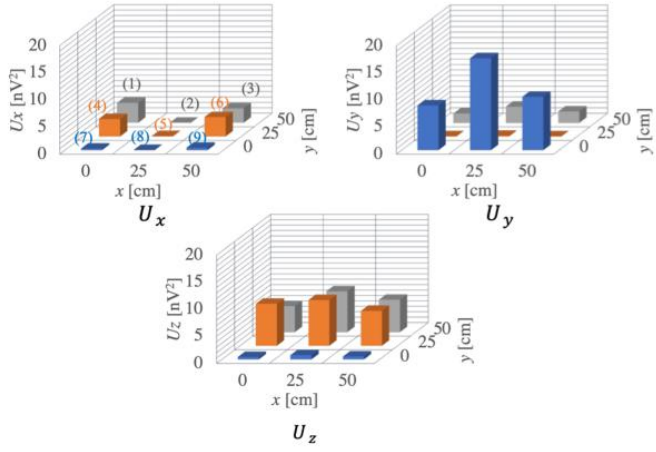

Fig. 8. Energy distribution of pulse electric field at the measurement plane 10 cm away from the vertical coupling plane. The ESD gun charging voltage is 4 kV.

phantom. The gel phantom was 30 cm long and 6 cm thick, and was equivalent to 2/3 times the dielectric properties of muscle [19]. On the other hand, three pairs of sensing electrodes were attached on the phantom surface to detect the pseudo myoelectric signals.

The detected myoelectric signals were first filtered and differentially amplified and then sent to the controller by wires to drive the artificial hand. The myoelectric artificial hand was set 10 cm away from the vertical coupling plane according to IEC61000-4-2, and was placed laterally or frontally facing the vertical coupling plane as shown in Fig. 10. As summarized in Table 2, the myoelectric artificial hand was set to open and grasp repeatedly, and each state of opening or grasping of the hand was maintained for 5 seconds. The malfunction of myoelectric artificial hand was defined as situations where it was not possible to maintain the state of being open or grasped for 5 seconds or to change from the opening/grasping state to the grasping/opening state of the hand smoothly. Such a malfunction is known as soft failure. The soft failure of ESD does not cause permanent damage (hard failure) to the devices. To increase test reliability, the myoelectric signals were acquired from 5 subjects and stored in the pseudo signal generator in advance. The hand movement was repeated 50 times in total for either lateral or front orientation. The ESD immunity test conditions were the same as in Table I.

TABLE II
MOVEMENT OF MYOELECTRIC ARTIFICIAL HAND

Number of subjects	5
Hand movement	Open and grasp
Duration in each state	5s
Total number of hand movement	50

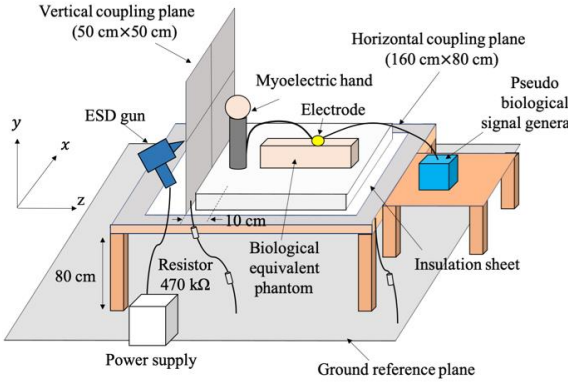

Fig. 9. Immunity test environment of wired myoelectric artificial hand.

Fig. 11 shows the measurement results of malfunction rate at the three positions when the myoelectric artificial hand was laterally facing and frontally facing the vertical coupling plane, respectively, under the ESD gun charging voltage of ±4 kV. When the myoelectric artificial hand was placed laterally facing the vertical coupling plane, the malfunction rate was 37%, 31% and 34% from the left position to right position. When the myoelectric artificial hand was placed frontally facing the vertical coupling plane, the malfunction rate was 30%, 32% and 33% from the left position to right position. When the ESD gun charging voltage was changed to ±2 kV, the trend of malfunction rate by positions was similar. For example, the malfunction rate when laterally placing the myoelectric artificial hand was 10%, 7% and 9% from the left position to the right position. Therefore, the malfunction rate varies depending on the placement of the myoelectric artificial hand, but the difference from the placement is not so large. The highest malfunction rate was found when the myoelectric artificial hand was placed laterally on the left side of the vertical coupling plane. It can be considered as a preferred placement of the myoelectric artificial hand to perform the worst case test.

C. Coupling Location of ESD Noise

From the immunity test results, we confirmed that the malfunction rate of myoelectric artificial hand varies slightly depending on the position and orientation of placement. In this subsection, we attempted to identify the location of ESD noise coupling into the myoelectric artificial hand and to examine which parameter of ESD-generated pulse is more correlated with the malfunction of myoelectric artificial hand.

It is not difficult to imagine that the wires between the myoelectric signal detector and the motor controller is one of paths that pick up ESD noise. To clarify this point, we attached some ferrite cores to these wires during the immunity test. Fig. 12 shows the measurement environment with ferrite cores attached to the wires between the myoelectric signal detector and the motor controller. The only difference from the immunity test in the previous subsection was the attachment of the ferrite cores. The myoelectric artificial hand was placed in the same three positions with lateral orientation.

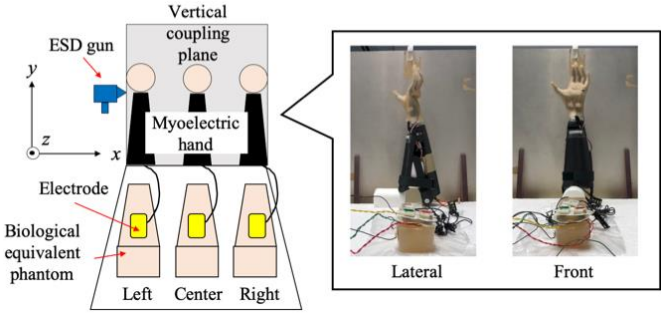

Fig. 10. Placement of myoelectric artificial hand.

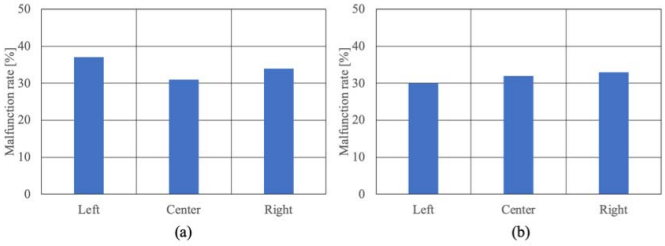

Fig. 11. (a) Malfunction rate when the myoelectric artificial hand is laterally facing the vertical coupling plane. (b) Malfunction rate when the myoelectric artificial hand is frontally facing the vertical coupling plane. The ESD gun charging voltage is 4 kV.

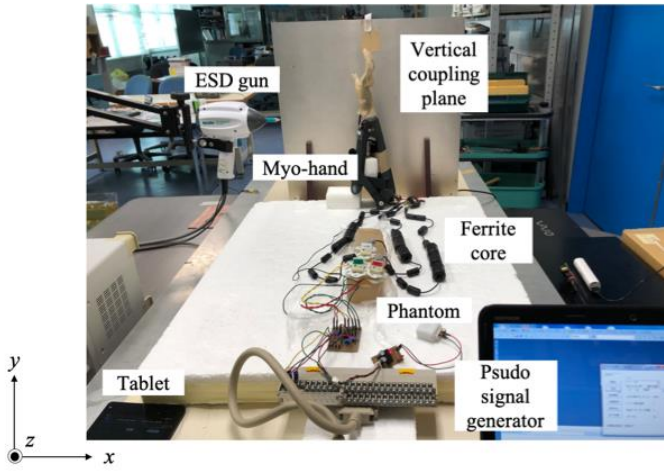

Fig. 12. Immunity test environment of wired myoelectric artificial hand with ferrite core attachment.

Fig. 13 shows the measured malfunction rate to be 10%, 7% and 9% from left position to the right position. Compared to Fig. 11 (a), which has the same test conditions except for the presence of ferrite cores, the malfunction rate was reduced by approximately

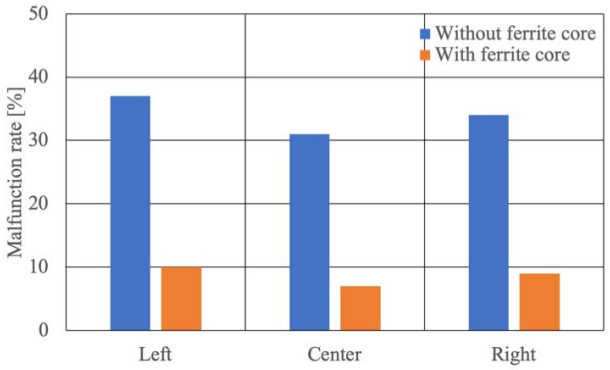

Fig. 13. Malfunction rate when the myoelectric artificial hand is laterally facing the vertical coupling plane and the ferrite cores are attached or not attached to the wires between the myoelectric signal detector and the motor controller. The ESD gun charging voltage is ±4 kV.

30% by ferrite core attachment. This result suggests that most of the ESD noise was coupled from the wires between the myoelectric signal detector and the motor controller, and the effect is so large that it explains the main cause of malfunction.

In addition, based on the results of electric field measurement and immunity test, we investigated which parameter of the ESD-generated pulse electric field is dominate to the malfunction rate of myoelectric artificial hand. We calculated the correlation coefficients between the peak level, time duration, energy of ESD-generated pulse and the malfunction rate of myoelectric artificial hand for the 9 measurement positions at the vertical measurement plane 10 cm or 45 cm away from the vertical coupling plane. The ESD gun charging voltages were ±2 and ±4 kV, respectively. As a result, the highest correlation coefficient of 0.88 was found between the z-directed peak electric field level E_{Pz} at the measurement positions in the lower part of the measurement plane and the malfunction rate of myoelectric artificial hand. This finding is consistent with the fact that the ESD-generated pulse noise is mixed into the myoelectric artificial hand through wires along the arm phantom on the wooden table. Since E_{Pz} is parallel to the wires, the wires may act like antennas to pick up the noise.

IV. ESD Immunity Performance Improvement By Wireless Control

A. Wireless Myoelectric Artificial Hand

Although a myoelectric artificial hand with internal wired connections is the current mainstream, wireless connections are highly expected for convenience. From the point of views that myoelectric artificial hands support user's daily life, high immunity performance is essential, so removing the wires between the myoelectric signal detector and the motor controller may be effective. We therefore developed a wireless myoelectric artificial hand [16]. Fig. 14 shows a block diagram of the wireless myoelectric artificial hand. The myoelectric signals are acquired using three pairs of sensing electrodes. Then the acquired myoelectric signals are converted into digital signals and modulated in an HBC based transmitter [16][17]. The human body itself acts as a communica-

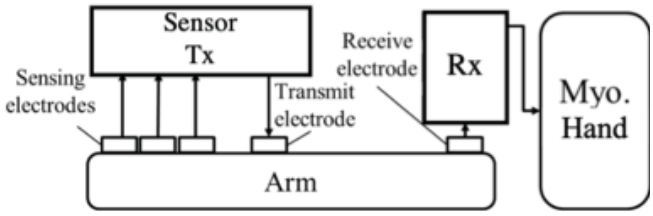

Fig. 14. Block diagram of wireless myoelectric artificial hand.

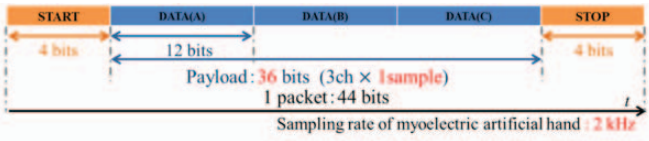

Fig. 15. Packet configuration.

tion route instead of the wires, which contributes to low path loss and high reliability. To transmit the three channels of myoelectric signals sampled with 2 kHz and 12 bit quantization in the ADC, the packet is configured as in Fig. 15. Before and after the payload of 36 bits (3 channels × 12 bits), four start bits and stop bits are added respectively. The packet rate is set to 2 kHz. In order to avoid superimposing this frequency component on the myoelectric signals in the range below 500 Hz, a low pass filter (LPF) with 500 Hz cutoff frequency is inserted to eliminate this influence.

The modulation employs an impulse radio multi-pulse position modulation (IR-MPPM) scheme in the 10 - 50 MHz band. It expresses information bits by temporally arrangement of multiple pulses. As shown in Fig. 16, we use 8 pulses to represent one digital information bit. The pulse width is 100 ns and the bit width is 800 ns. So the data rate is 1.25 Mbps. This wideband modulation scheme is particularly resistant to ESD-type impulse noises because it can be demodulated from other remaining pulses even if one or two pulses are interfered. The demodulation method is energy detection. As shown in Fig. 17, we first summarize the total energy in the specific time intervals. Then we compare the two energy values. If the total energy 2 is larger than the total energy 1, the corresponding digital information bit is "0". Conversely, if the total energy 1 is larger than the total energy 2, the corresponding digital information bit is "1". This demodulation method does not require a threshold to determine the bit of "0" and "1", and is implemented in a field programmable gate array (FPGA) evaluation board (Xilinx, Virtex-6).

B. Immunity Test Environment

The ESD immunity tests were performed under the same conditions for the wired and wireless myoelectric artificial hand according to IEC61000-4-2 in order to compare their malfunction rates. Based on the previously result, the myoelectric artificial hand was placed laterally on the left side. All circuits and equipment used for test, such as the transceivers, the pseudo myoelectric signal generator, and a PC for FPGA control, were driven by batteries to reduce unnecessary common mode noise influence. Table III shows the ESD immunity test conditions, and Fig. 18 shows the outline of the immunity test for the wired and wireless myoelectric artificial hand. A scene of the test for wireless myoelectric artificial hand is shown in Fig. 19. Although the time interval of discharge was set to 0.05 s in the previous section, the one second interval was recommended here in order to approximate a more realistic environment. The ESD charging voltage is specified as _2, 4, 6, 8 kV in the IEC61000-4-2 standard, but in this test the charging voltage was set to _1, 2, 3, 4, 6, 8 kV for being easy to compare the trend of malfunction. The movement of the myoelectric artificial hand is the same as in Table II, and the definition of malfunction is also the same as in the previous section.

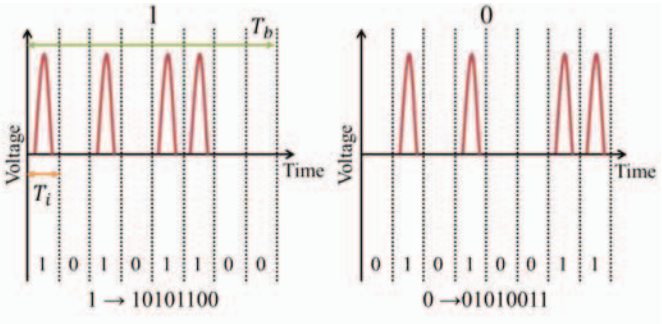

Fig. 16. IP-MPPM modulation.

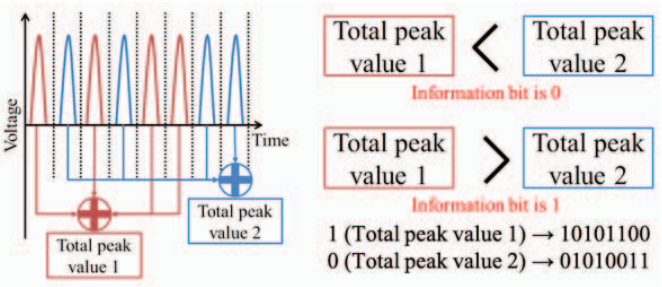

Fig. 17. Energy detection demodulation.

TABLE III
ESD IMMUNITY TEST CONDITIONS FOR WIRELESS MYOELECTRIC ARTIFICIAL HAND

Discharge method	Contact discharge
Charging voltage	±1, 2, 3, 4, 6, 8 kV
Coupling plane	Vertical plane
Time interval of discharge	1 s
Number of discharge	50

C. ESD Immunity Test Results

Fig. 20 shows the malfunction rate as a function of ESD gun charging voltage. As can be seen, the malfunction rate increased as the charging voltage increased for both wired and wireless myoelectric artificial hand. It should be noted that the malfunction rate was lower than that shown in Fig. 13 at the same ±4 kV charging voltage because the time interval of discharge was increased from 0.05 s to one second. When the ESD charging voltage was 8 kV, the malfunction rate for wired control was approximately 35%, but it was reduced to approximately 15% for wireless control, confirming that the malfunction rate was improved by 20%. From the test results, it was confirmed that there are two types of malfunctions of myoelectric artificial hand. One is when the operation is performed by mistake. This is because the myoelectric signal is

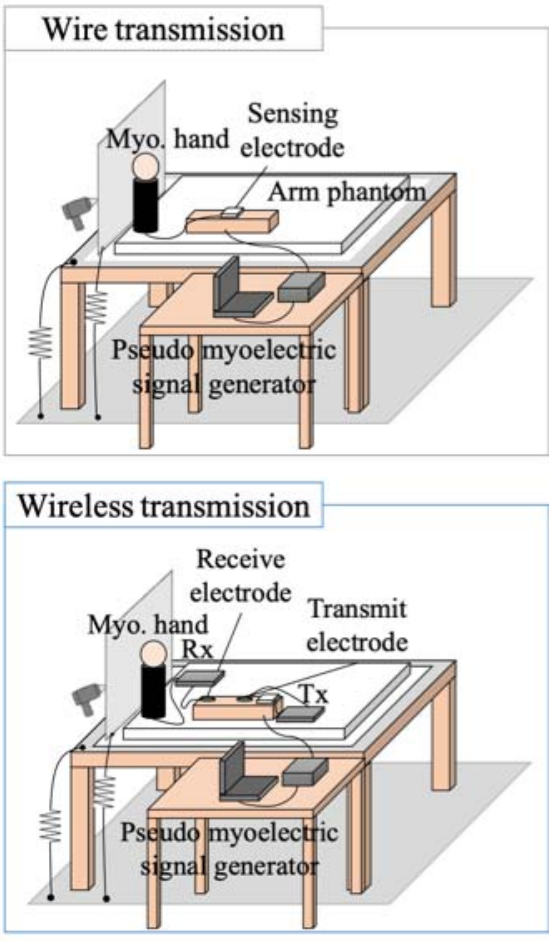

Fig. 18. ESD immunity test environment for the wired and wireless myoelectric artificial hand.

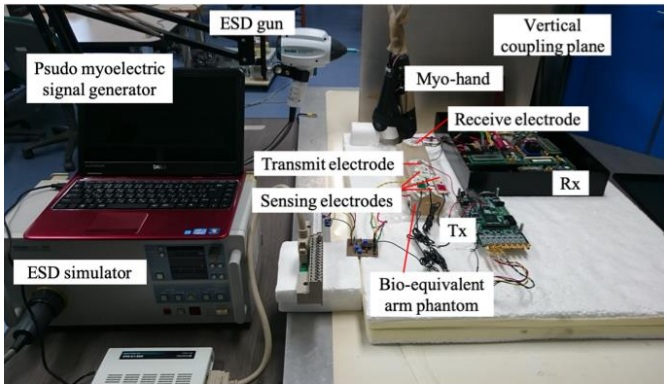

Fig. 19. A scene of ESD immunity test of wireless myoelectric artificial hand.

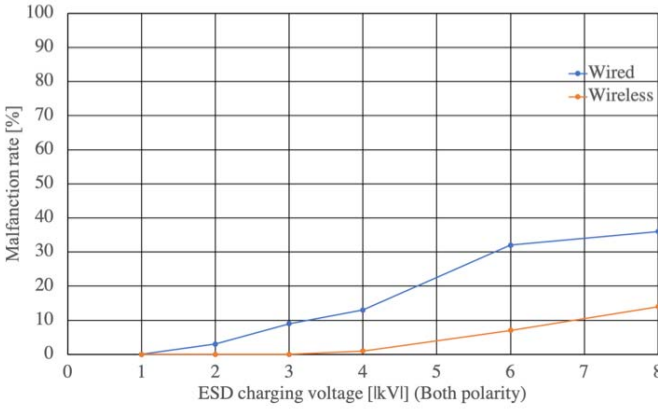

Fig. 20. Malfunction rate versus ESD gun charging voltage.

coupled with ESD noise and the myoelectric artificial hand recognizes the wrong signal. The other is a malfunction which stops for a moment during operation. This may be because the PWM signal which controls the myoelectric artificial hand is directly affected by the noise coupled into the controller circuit. The former malfunction was confirmed especially in the wired control case, and it was thought that the ESD noise was superimposed through the wires between the myoelectric signal detector and the motor controller. That is the reason why the malfunction rate of wired control was high. On the other hand, by adopting the wideband IR-MPPM modulation scheme which is especially resistant to impulse noise and an energy detection method which compares the energy of multiple pulses, the possibility of bit errors occurring in wireless control was significantly reduced. This is considered to be the major factor which improved the malfunction rate by 20% compared to wired control.

V. Conclusion

In this study, focusing on a myoelectric artificial hand as a wearable robot, we have performed ESD immunity tests based on the IEC61000-4-2 standard and clarified the mechanism of malfunction against ESD noise. From the results of electric field measurement and immunity test, we have analyzed the correlation between the peak level, time duration, energy of ESD-generated pulse electric field and the malfunction rate of the myoelectric artificial hand. It has been clarified that the peak electric field level has the highest correlation with malfunction. In addition, it has been confirmed that the ESD noise is coupled into the wires between the myoelectric signal detector and the motor controller, and replacing the wires with an HBC-based wireless transceiver has shown a higher immunity level for ESD-type impulse noise. This is because the wires pick up noise and the wireless transceiver with a wideband modulation scheme is strong against the ESD-type impulse noise. As a result, the malfunction rate of myoelectric artificial hand with wireless control has been improved by 20% compared to wired control.

The future subject is to establish a standard immunity test method for various increasing wearable robots. Based on some documents [6] submitted to a working group of the International Electrotechnical Commission (IEC) International Special Committee on Radio Interference (CISPR), a discussion on methods to test the immunity of a wearable robotic equipment has been initialized, and the IEC Advisory Committee on Electromagnetic Compatibility is advising the Technical Committee TC62/SC62D in charge of medical electronic devices to investigate the possible immunity methods.

References

[1] J. Wang and Q. Wang, Body Area Communication, Wiley-IEEE, 2012.
[2] F. Chen, Z. Li, C.L.P. Chen, and S. Agaian, "Introduction to the special issue on

human cooperative wearable robotic systems," IEEE Robot. Autom. Lett., vol. 3, no. 1, pp. 466-468, Jan. 2018.
[3] L. Randazzo, I. Iturrate, S. Perdikis, and J. d. R. Millan, "mano: A wearable hand exoskeleton for activities of daily living and neurorehabilitation," IEEE Robot. Autom. Lett., vol. 3, no. 1, pp. 500-507, Jan. 2018.
[4] T. Seki, T. Nakamura, R. Kato, S. Morishita, and H. Yokoi, "Development of five-finger multi-DoF myoelectric hands with a power allocation mechanism," J. Mechanics Eng. and Automation, vol.4, pp. 97-105, Feb. 2014.
[5] C. Ji, D. Anzai, J. Wang, I. Mori, and O. Fujiwara, "An ESD immunity test for battery-operated control circuit board in myoelectric artificial hand system," IEICE Trans. Commun., vol. E98-B, no.12, pp. 2477-2484, Dec. 2015.
[6] J. Wang, D. Anzai, O. Fujiwara, Y. Kami, T. Ishida and F. Amemiya, "A report of ESD immunity testing relating to body worn equipment using robotic technology including electro-technology," CISPR/I/WG4 Contribution, 17-01, Feb. 2017.
[7] J. Wang, R. Nakaya, K. Sato, D. Anzai, O. Fujiwara, and F. Amemiya, "Development of an immunity test system with a pseudo biosignal generator for wearable devices and application to the ESD test of an artificial hand," IEEE Trans. Electromagn. Compat., vol. 61, no. 1, pp. 73-81, Feb. 2019.
[8] T. Ishida, S. Nitta, F. Xiao, Y. Kami, and O. Fujiwara, "An experimental study of electrostatic discharge immunity testing for wearable devices," in Proc. IEEE Int. Symp. on Electromagn. Compat., Dresden, Germany, Aug. 16-22, 2015, pp. 839-842.
[9] T. Ishida, F. Xiao, Y. Kami, O. Fujiwara, and S. Nitta, "Characteristics of discharge currents measured through body-attached metal for modeling ESD from wearable electronic devices," IEICE Trans. Commun., vol. E99-B, no. 1, pp. 186?191, Jan. 2016.
[10] M. Kohani, A. Bhandare, L. Guan, D. Pommerenke, and M. G. Pecht, "Evaluating characteristics of electrostatic discharge (ESD) events in wearable medical devices: Comparison with the IEC 61000-4-2 standard," IEEE Trans. Electromagn. Compat., vol. 60, no. 5, pp. 1304-1312, Oct. 2018.
[11] W. Liao, K. Nagai, and J. Wang, "An evaluation method of electromagnetic interference on bio-sensor used for wearable robot control," IEEE Trans. Electromagn. Compat., DOI: 10.1109/TEMC.2019.2896974, Feb. 2019.
[12] T. Yoshida, "A study on electrical stress induced by electrostatic discharge on wearable devices," in Proc. 7th Asia-Pacific Conf. on Environmental Electromagn., Hangzhou, China, Nov. 4-7, 2015, pp. 230-233.
[13] T. G. Zimmerman, "Personal area networks: Near-field intrabody communications," IBM Syst. J., vol. 35, no. 3&4, pp. 609-617, 1996.
[14] H. Baldus, S. Corroy, A. Fazzi, K. Klabunde, and T. Schenk, "Humancentric connectivity enabled by body-coupled communications," IEEE Commun. Mag., vol. 47, no. 6, pp. 172-178, June 2009.
[15] J. Wang, T. Fujiwara, T. Kato, and D. Anzai, "Wearable ECG based on impulse radio type human body communication," IEEE Trans. Biomed. Eng., vol.63, no.9, pp.1887-1894, Sept. 2016.
[16] H. Ando, Y. Murase, D. Anzai, and J. Wang, "Wireless control of robotic artificial hand using myoelectric signal based on wideband human body communication," IEEE Access, vol. 7, pp. 10254-10262, Jan. 2019.
[17] J. Wang, "Wide band human body communication technology for wearable and implantable robot control," IEICE Trans. Commun., vol. E103-B, no.6, pp 628-636, June 2020.
[18] International Electrotechnical Commission, IEC 61000-4-2, Electromagnetic compatibility (EMC) - Part 4-2: Testing and measurement techniques - Electrostatic discharge immunity test, Edition 2.0, IEC 61000-4-2, Dec. 2008.
[19] K. Ito, H. Kawai, and K. Saito, "State of the art and future prospects of biological tissue-equivalent phantoms," Trans. IEICE, vol. B85, no. 5, pp. 582-596, May 2002.

Biographies

Yasuhiro Morinaga *received the B.E. degree in electrical and electronic engineering from the Nagoya Institute of Technology, Nagoya, Japan, in 2019. He is currently engaged in ESD immunity evaluation of wearable devices towards the M. E. degree also at the Nagoya Institute of Technology, Japan.*

Keinosuke Nagai *received the B.E. and M.E degrees in electrical and electronic engineering from the Nagoya Institute of Technology, Nagoya, Japan, in 2017 and 2019, respectively. During his time as a graduate student at Nagoya Institute of Technology, he was involved in the ESD immunity evaluation of wearable devices. He is currently with Toyota Industries Corporation, Japan.*

Jianqing Wang *(M'99, SM'19, F'21) received the B.E. degree in electronic engineering from the Beijing Institute of Technology, Beijing, China, in 1984, and the M.E. and D.E. degrees in electrical and communication engineering from Tohoku University, Sendai, Japan, in 1988 and 1991, respectively. He was a Research Associate with Tohoku University, and a Senior Engineer with the Sophia Systems Co. Ltd. In 1997, he joined the Nagoya Institute of Technology, Nagoya, Japan, where he has been a Professor since 2005. He authored Body Area Communications (Wiley-IEEE) in 2012, and received the IEEE EMC Society Technical Achievement Award in 2019. His current research interests include biomedical communications and electromagnetic compatibility.*

Daisuke Anzai *(S'06-M'11) received the B.E., M.E., and Ph.D. degrees from Osaka City University, Osaka, Japan, in 2006, 2008, and 2011, respectively. Since 2011, he has been with the Graduate School of Engineering, Nagoya Institute of Technology, Nagoya, Japan, where he is currently an Associate Professor. His current research interests include biomedical communication systems and localization systems in wireless communication networks. Dr. Anzai was a recipient of the 2015 IEEE MTT-S Japan Young Engineer Award and the Telecommunications Technology Award from the Telecommunications Advancement Foundation.* **EMC**